CONFERENCE PRE-PRINT

THE X-POINT RADIATOR REGIME IN THE WEST TOKAMAK FOR DIVERTOR OPERATION IN NEXT STEP FUSION DEVICES

N. RIVALS

CEA, IRFM

Saint-Paul-lez-Durance, France

Email: nicolas.rivals@cea.fr

N. FEDORCZAK, E. GEULIN, R. NOUAILLETAS, D. MOIRAF, C. GUILLEMAUT, J.P. GUNN, J. MORALES, P. MANAS, L. FEVRE, A. EKEDAHL, J. GERARDIN, Y. CORRE, P. MAGET, E. TSITRONE CEA, IRFM

Saint-Paul-lez-Durance, France

H. YANG

Aix-Marseille Univ., CNRS, Centrale Med., M2P2 Marseille, France

P. HENNEQUIN

Laboratoire de Physique des Plasmas, CNRS, Sorbonne Université, École polytechnique, Institut Polytechnique de Paris Palaiseau, France

J. GASPAR

Aix-Marseille Univ., CNRS, IUSTI Marseille, France

M. BERNERT, T. LUNT

Max Planck Institute for Plasma Physics

Garching, Germany

S. HENDERSON

United Kingdom Atomic Energy Authority, Culham Centre for Fusion Energy, Culham Science Centre Abingdon, UK

H. REIMERDES

Ecole Polytechnique Fédérale de Lausanne (EPFL), Swiss Plasma Center (SPC) Lausanne, Switzerland

N. VIANELLO

Consorzio RFX

Padova, Italy

The EUROfusion Tokamak Exploitation Team

See the author list of E. Joffrin et al 2024 Nucl. Fusion 64 112019

The WEST team

See http://west.cea.fr/WESTteam

Abstract

From 2023 to 2025, the WEST tokamak featuring a full tungsten environment and ITER-grade divertor plasma-facing components ran in-depth studies of L-mode X-Point Radiator (XPR) experiments. This potentially reactor-relevant regime aims at addressing the power exhaust challenge in fusion power plants, mitigating heat loads, material erosion and impurity plasma contamination. A database of 129 XPR pulses was constituted, with varying density, input power, plasma currents, and magnetic configurations. The XPR regime is characterised in WEST: nitrogen seeding induces the onset of a characteristic stable MARFE at the X-Point, associated with a sharp transition of the divertor plasma to cold (~ 3 eV) and dense conditions. In this state, the electron temperature drops abruptly (T_e cliff) at the outer target, with still significant particle fluxes. Divertor

tungsten sources are strongly reduced, up to a 50-fold reduction, and core plasma performance is improved. This regime was successfully and repeatably real-time controlled with a simple interferometry line-of-sight observable. This allowed to run long pulses, and a 34 second continuously sustained XPR was achieved. They have been found to be very stable in the so-called "favourable" magnetic configuration, while in unfavourable configuration the X-Point MARFE destabilizes and is more prone to disrupt the plasma. This behaviour has been reproduced in numerical boundary simulations with the SOLEDGE3X code, highlighting the importance of the ExB drifts flows and direction.

1. INTRODUCTION

The divertor of next step fusion devices such as in ITER and DEMO must survive years of quasi-continuous operation, and thus requires the divertor plasma to be cooled and controlled below 5 eV on the target plates, to prevent excessive tungsten erosion and plasma contamination. To anticipate this challenge, an ITER-grade divertor has been deployed in the WEST tokamak [1], and impurity-seeded plasmas were executed to reach such divertor plasma conditions. Those scenarios take the form in WEST of so-called "X-Point Radiator" (XPR) scenarios, featuring a stable radiation ring (MARFE) at the X-Point, similarly to scenarios obtained in other machines such as ASDEX-Upgrade [2], JET [3], MAST-U [4], DIII-D [5], and TCV [6]. The WEST tokamak, from its ability to run very long discharges [7] thanks to its full-tungsten and actively cooled environment, brings a new angle on those experiments: long pulse XPR scenarios (several tens of seconds), and in different magnetic configurations (Lower Single Null "LSN", Upper Single Null "USN", and Double Null "DN").

2. FEATURES OF THE WEST X-POINT RADIATOR REGIME

In WEST, XPR regimes are produced by injection of nitrogen in L-mode scenarios. Upon sufficient seeding, the WEST divertor plasma, which is initially hot ("attached plasma") with electron temperatures in the 20 to 40 eV range, eventually transitions into a cold (< 3 eV) and dense ($n_e \sim 8\text{-}10 \times 10^{19} \text{ m}^{-3}$) plasma at the divertor targets, with mitigated heat loads by factors of ~10, but with still equivalent ion flux to the divertor targets [8]. This condensation of the divertor plasma coincides with the appearance of the characteristic stable toroidal radiation ring (MARFE) just above the X-Point, from where the name "X-Point Radiator" stems.

An example of the two divertor plasma states, "attached scenario" (without seeding) vs. "XPR scenario" is illustrated in Fig. 1. Before the onset of the XPR (in red), the electron temperature profile at the divertor targets shows peaks at the inner and outer magnetic strike points, at around $20 \, \text{eV}$. After the onset of the XPR (in blue), the T_e profile becomes uniformly flat at $3-4 \, \text{eV}$ all along the surface. Particle fluxes still remain important, meaning the underlying process of the XPR transition in WEST is not plasma "detachment" in the usual sense involving the decrease of particle fluxes, such as in the "degree-of-detachment (DoD)" definition [9]. The shape of the profile does change before and after the transition, with an outward shift of the peak by a few centimetres on the outer side. However, after the initial formation of the XPR and with further seeding, particle fluxes do start to decrease, leading then to particle detachment. This sequence is illustrated in Fig. 2., which shows time traces of plasma parameters from Langmuir probe measurements at the inner and outer strike points, during a prescribed nitrogen seeding ramp. With the initial injection of nitrogen, the outer target electron temperature is roughly unchanged, until the XPR formation where an abrupt decrease to 3-5 eV occurs. This so-called " T_e cliff" is only observed on the outer side, as the inner side shows a gradual decrease to cold temperature, without discontinuity. The electron density spikes and then further decreases, with still constant and cold temperatures, resulting in an increase of the Degree-of-Detachment (third row).

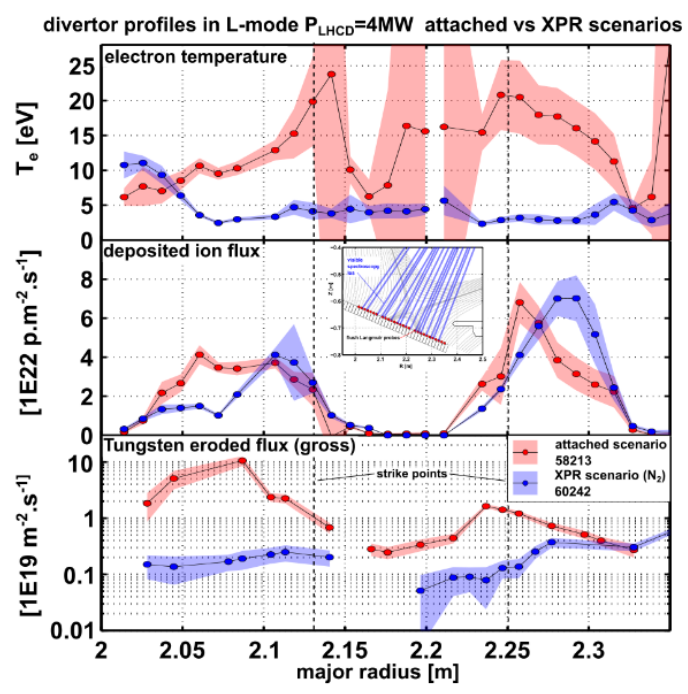


FIG 1: Comparison of WEST divertor target electron temperature, particle fluxes, and tungsten eroded flux profiles for a standard "attached" plasma scenario (red) and an XPR scenario (blue). Tungsten eroded flux are estimated using S/XB atomic data from [11].

The time scales involved in the XPR formation at the time of the T_e cliff are very short with respect to the pulse length, and multiple time scales exist: fast acquisition Langmuir probes at the divertor surface show a drop in electron temperature within a few microseconds [10], while fast visible camera imaging tracking the movement of the radiation front shows its movement from the target to above the X-Point in a few milliseconds [12].

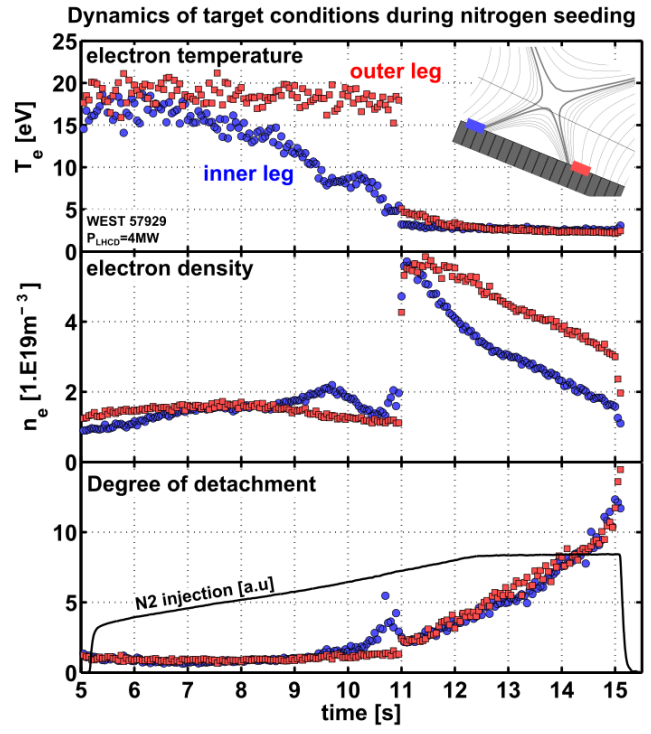


FIG 2: WEST divertor target time traces for electron temperature, electron density, and degree of detachment (DoD) during a prescribed nitrogen seeding ramp.

The third row of Fig. 1. shows the tungsten gross eroded flux calculated from the visible spectroscopy signal at 400.9 nm with the associated S/XB coefficients [11]. After the condensation into the cold divertor state, W sources are strongly tamed, with a reduction by a factor of 50 at the inner target and factor of 20 at the outer target.

Core plasma performance improves upon nitrogen injection with significant increases of core confinement (τ_E +25%, from ion dilution effects [13]), central T_e (+20%), and T_i (+35%), and those benefits remain through the transition to the XPR state. Such improvements are concomitant effects of reduced W contamination from tamed divertor sources. At the same time a significant enhancement of the edge rotation is observed from Doppler Back Scattering measurements [14] as shown in Fig. 4, consistent with edge transport reduction. Also notably, upon the XPR onset, the poloidal flows in the SOL outside the separatrix vanishes, which could be considered an effect of the re-symmetrisation of targets profiles. This has implications for eroded impurity migration and redeposition pattern studies.

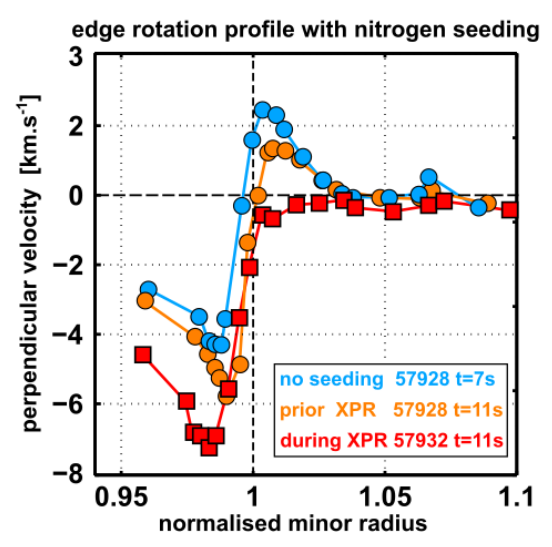


FIG 3: Perpendicular $(E \times B)$ rotation profile from Doppler Backscattering, compared between no-nitrogen (blue), with nitrogen but before the XPR onset (orange), and during XPR regime (red).

Main chamber midplane SOL profiles, measured from reciprocating Langmuir Probes plunges, are only weakly impacted by the onset of XPR's. As a consequence, Radio-Frequency (RF) heating coupling is preserved, and at the same time, potential plasma-wall interactions at the first wall and antennas and associated tungsten sources remain the same, in contrast to divertor sources which are reduced.

3. XPR SCENARIO CONTROL

A clear marker of the XPR transition in WEST can be identified on the line-integrated density measured by interferometry on the line-of-sight passing through the X-Point, as illustrated in the yellow curve in Fig. 4. With nitrogen seeding, the X-Point density signal first grows steadily, until a very sharp drop, which coincides with the movement of the radiation from the target to the X-Point. This phenomenon consistently marks the onset of the XPR regime in WEST. Following this drop, further increase in nitrogen seeding up to radiative collapse induces a monotonic increase of this observable (from "2" to "3" in the middle row of Fig. 4), which makes this signal a possible observable for a control system for the phase after the XPR onset. The interpretation of this density drop and increase is further discussed in the next section.

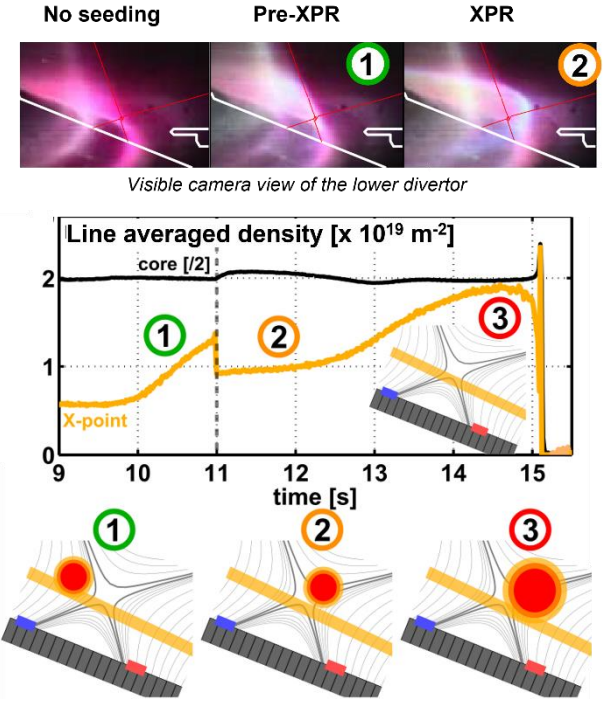


FIG 4: Comparison of the different states in the XPR formation, from the no-seeding phase (top left) to "deep" XPR close to radiation collapse (number "3"). First row: visible camera image, middle row: line-averaged densities from interferometry lines of sight passing though of core (black), and passing through the X-Point (orange). The line of sight passing through the X-Point is represented in the bottom row, with an illustration of the estimated location and spatial extension of the plasmadense MARFE, for interpretative purposes of the time traces above.

A real-time control scheme was developed using the seeding rate as actuator, in which the latter is automatically adjusted so that the X-Point density reaches a prescribed value, while the deuterium fueling remains tied to the central interferometry line of sight controller. With this control scheme, the XPR regime was successfully and repeatably stabilized, as illustrated in Fig. 5. The XPR transition is executed during the initial ramp, and then sustained for the flat-top phase, where the seeding rate shows an exponential decay time of the order of 5 seconds, due to wall loading effects and slow pumping. In this scenario, the XPR holds for a few seconds after the seeding stops, before re-attaching and in a cleaning phase, enabling plasma landing with low disruptivity and the control of nitrogen legacy without resorting to post-pulse cleaning schemes.

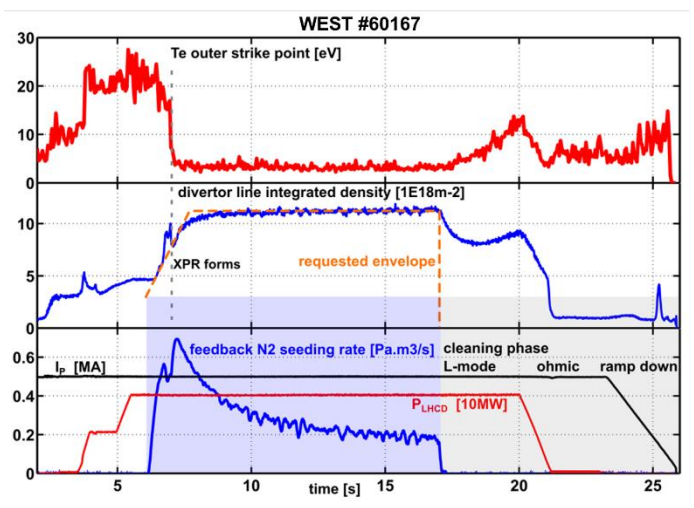


FIG 5: Illustration of real-time control of the XPR regime in WEST pulse #60167, with time traces of the outer target electron temperature (top row), line integrated density from the line of sight passing through the X-Point (middle row) as observable (blue trace) and requested envelope in the real-time control system (dashed orange). The nitrogen seeding rate (actuator) is plotted in blue in the bottom row, along with plasma current (black), and injected power (red).

Using this control scheme, a 34 second-long XPR phase was sustained in WEST pulse #62352, which featured similar particle fluxes as in attached scenarios. This forms now the basis for testing the WEST divertor ITER-grade plasma facing components (PFC) in more ITER relevant conditions: i.e., at high particle fluence and sub-10 eV temperatures (vs. high particle fluence at $T_e > 20 \text{ eV}$ in previous high fluence campaigns [15]).

The possibility of using such a simple interferometry signal as a reliable control scheme for XPR regimes also opens new sensor and control perspectives for next step fusion devices where sensor possibilities may be limited [16].

4. WEST XPR DATABASE

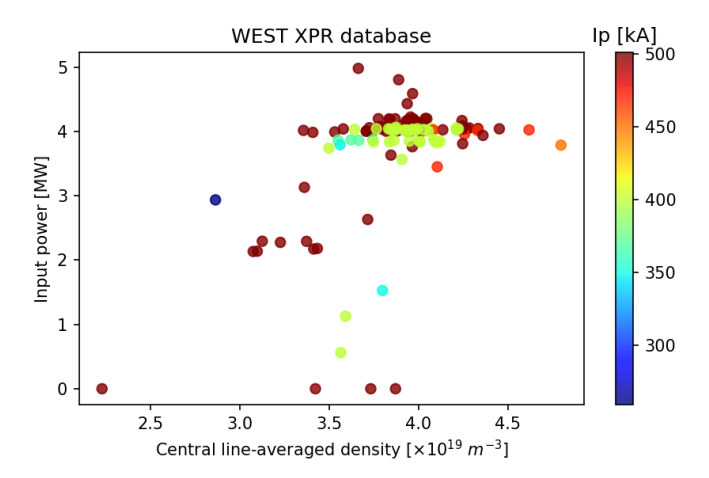


FIG 6: Summary of the 129 pulses in the WEST XPR pulse database, as a function of density, auxiliary injected power, and plasma current.

XPR scenarios in WEST have been found to be stable and controllable over a range of density $\langle n_e \rangle \sim 2.5 - 4.5$ m^{-2} , input power from $P_{IN} \sim 0.5$ (ohmic) to 5 MW, and plasma currents from 250 to 500 kA. The constructed WEST XPR database now features 129 nitrogen pulses as shown in Fig. 6, and includes different magnetic configurations in which XPR stability varies significantly. In Lower Single Null (LSN) magnetic configuration with $B \times \nabla B$ drift towards the lower divertor where the active X-Point is (i.e., "favourable" configuration), nitrogen seeding induces the following sequence of events: first, the High Field Side (HFS) target plasma turns cold and dense, with the appearance of the MARFE there, reminiscent of the so-called "High Field Side High Density (HFSHD) front" as seen in ASDEX-Upgrade [17]. With further seeding, and when the outer target also becomes cold, the MARFE jumps horizontally from the HFS above the X-Point, as illustrated in the lower row of Fig. 4. Attempts to trigger such regimes in Upper-Single Null (USN), which corresponds to the "unfavourable" configuration in WEST, leads to a different behaviour. First, a similar HFSHD front appears, but instead of moving horizontally to a stable position at upper X-Point, it either leads to a dynamic MARFE moving towards the bottom of the machine (i.e., on the opposite side of the active X-Point), or to a disruption. This effect is illustrated in the image from the visible camera left of Fig. 7, and is reproduced with boundary simulations with the SOLEDGE3X code including cross-field drifts, where a reversal of the toroidal field triggers fast movement of the MARFE away from the active X-Point (right side of Fig. 7). This highlights the importance of the direction of drift flows to accurately describe the transition dynamics and stability in XPR scenarios. Since flows (and thus also drift flows) are also of high importance in material erosion, contamination and migration/redeposition matters, an accurate description of drifts in the boundary modelling brick of integrated models is necessary to reliably predict power plant performance from core to PFC's.

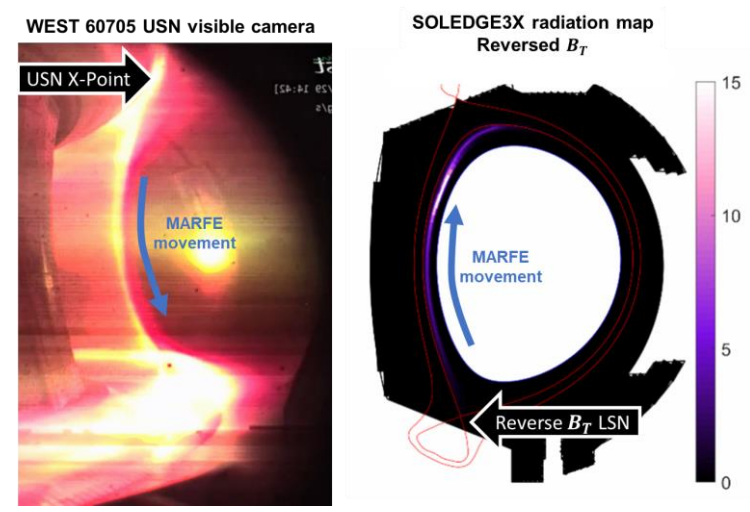


FIG 7: Illustration of the behavior of the XPR MARFE in unfavorable configuration (ion $B \times \nabla B$ drift away from the active X-Point) in WEST as an Upper Single Null scenario, with the X-Point MARFE moved to the opposite side of the X-Point), and on the right an equivalently unfavorable configuration in a SOLEDGE3X simulation with drifts, as an LSN but reversed toroidal field, with the MARFE moving upward, equivalent to the experimental observation.

5. CONCLUSION AND OUTLOOK

The XPR operational space has been explored in WEST full tungsten environment in L-mode scenarios. 129 successful XPR pulses were carried out in two years of experimental campaign, demonstrating the stability and reproducibility of such scenarios in WEST. They were successfully real-time controlled with a simple observable: an interferometry line-of-sight passing through the X-Point, a diagnostic potentially compatible with fusion power plant designs. In WEST, XPR scenarios produce both a cold divertor with high particle flux, tamed W divertor sources and an improved core confinement. As a consequence, this was chosen to be the scenario for the next high-fluence campaign at WEST to test the divertor ITER-grade PFC's by reproducing ITER divertor particle fluence with now also similar sub-10 eV plasma temperatures, and investigate residual tungsten erosion and migration.

ACKNOWLEDGEMENTS

This work has been carried out within the framework of the EUROfusion Consortium, funded by the European Union via the Euratom Research and Training Programme (Grant Agreement No 101052200 — EUROfusion). Views and opinions expressed are however those of the author(s) only and do not necessarily reflect those of the European Union or the European Commission. Neither the European Union nor the European Commission can be held responsible for them.

REFERENCES

- [1] J. Bucalossi et al., Nucl. Fusion, 64 (2024) 112022
- [2] M. Bernert et al., *Nucl. Fusion* **61** (2021) 024001
- [3] M. Wischmeier et al., J. Nuc. Mater. 463 (2015) 22-29
- [4] F. Federici et al., Nuc. Mater. Energy 43 (2025)
- [5] L. Wang et al., Nat. Commun. 12 (2021) 1365
- [6] K. Lee et al., Phys. Rev. Lett. 134 (2025) 185102
- [7] R. J. Dumont et al., EPJ web. Conf. (submitted 2025)
- [8] N. Rivals et al., Nuc. Mater. Energy 40 (2025) 101723
- [9] A. Loarte et al., Nucl. Fusion, 38 (1998) 3
- [10] F. Causa et al., PSI-26 conference poster (2024)
- [11] C.A. Johnson et al., Nucl. Fusion 63 (2023) 096017
- [12] L. Fèvre, et al. EPS-51 conference poster (2025)
- [13] P. Maget Plasma Phys. Controlled Fusion 64 (2022)
- [14] L. Vermare et al., *Nucl. Fusion* **62** (2022) 026002
- [15] J. Gaspar et al., Nucl. Mater. Energy 41 (2024) 101745
- [16] W. Biel et al., Fusion Eng. Des., 179 (2022) 113122
- [17] P. Manz et al., Nucl. Mater. Energy, 12 (2017) 1152-1156